Research paper

A potent antagonist antibody targeting connexin hemichannels alleviates Clouston syndrome symptoms in mutant mice

Yuanyuan Kuang[a,b,c,d,1], Veronica Zorzi[e,f,1], Damiano Buratto[a], Gaia Ziraldo[e,f], Flavia Mazzarda[e,g], Chiara Peres[e,h], Chiara Nardin[e,h], Anna Maria Salvatore[e], Francesco Chiani[e], Ferdinando Scavizzi[e], Marcello Raspa[e], Min Qiang[a], Youjun Chu[a], Xiaojie Shi[a], Yu Li[a,b,c,d], Lili Liu[a], Yaru Shi[a], Francesco Zonta[a], Guang Yang[a,*], Richard A. Lerner[a,k,*], Fabio Mammano[a,e,h,*]

[a] Shanghai Institute for Advanced Immunochemical Studies, ShanghaiTech University, Shanghai 201210, China
[b] School of Life Science and Technology, ShanghaiTech University, 201210 Shanghai, China
[c] Institute of Biochemistry and Cell Biology, Shanghai Institutes for Biological Sciences, Chinese Academy of Sciences, 200031 Shanghai, China
[d] University of Chinese Academy of Sciences, 100049 Beijing, China
[e] CNR Institute of Biochemistry and Cell Biology, 00015 Monterotondo, Italy
[f] Institute of Otorhinolaryngology, Università Cattolica del Sacro Cuore, 00168 Rome, Italy
[g] Department of Science, Roma3 University, 00146 Rome, Italy
[h] Department of Physics and Astronomy "G. Galilei", University of Padova, 35131 Padova, Italy
[k] Department of Chemistry, Scripps Research Institute, La Jolla, CA 92037, U.S.A.

ARTICLE INFO

ABSTRACT

Background: Numerous currently incurable human diseases have been causally linked to mutations in connexin (Cx) genes. In several instances, pathological mutations generate abnormally active Cx hemichannels, referred to also as "leaky" hemichannels. The goal of this study was to assay the *in vivo* efficacy of a potent antagonist antibody targeting Cx hemichannels.
Methods: We employed the antibody to treat Cx30$^{A88V/A88V}$ adult mutant mice, the only available animal model of Clouston syndrome, a rare orphan disease caused by Cx30 p.A88V leaky hemichannels. To gain mechanistic insight into antibody action, we also performed patch clamp recordings, Ca^{2+} imaging and ATP release assay *in vitro*.
Findings: Two weeks of antibody treatment sufficed to repress cell hyperproliferation in skin and reduce hypertrophic sebaceous glands (SGs) to wild type (wt) levels. These effects were obtained whether mutant mice were treated topically, by application of an antibody cream formulation, or systemically, by intraperitoneal antibody injection. Experiments with mouse primary keratinocytes and HaCaT cells revealed the antibody blocked Ca^{2+} influx and diminished ATP release through leaky Cx30 p.A88V hemichannels.
Interpretation: Our results show anti-Cx antibody treatment was effective *in vivo* and sufficient to counteract the effects of pathological connexin expression in Cx30$^{A88V/A88V}$ mice. *In vitro* experiments suggest antibodies gained control over leaky hemichannels and contributed to restoring epidermal homeostasis. Therefore, regulating cell physiology by antibodies targeting the extracellular domain of Cxs may enforce an entirely new therapeutic strategy. These findings support the further development of antibodies as drugs to address unmet medical needs for Cx-related diseases.
Fund: Fondazione Telethon, GGP19148; University of Padova, SID/BIRD187130; Consiglio Nazionale delle Ricerche, DSB.AD008.370.003\TERABIO-IBCN; National Science Foundation of China, 31770776; Science and Technology Commission of Shanghai Municipality, 16DZ1910200.

Lead Contact: Fabio Mammano, fabio.mammano@cnr.it
* Corresponding Authors. Professor Fabio Mammano. Consiglio Nazionale delle Ricerche, Italy.
 E-mail addresses: yangguang@shanghaitech.edu.cn (G. Yang), rlerner@scripps.edu (R.A. Lerner), fabio.mammano@cnr.it (F. Mammano).
[1] Y.K. and V.Z. contributed equally to this work.

1. Introduction

Mutations in the Cx gene family can cause a variety of currently incurable human diseases ranging in severity from mild to fatal [1].

Research in context

Evidence before this study

There is an impelling need to develop specific and effective remedies for the numerous human diseases caused by Cx gene mutations. In prior work, we identified and characterized an anti-Cx antibody that is effective against abnormally active Cx hemichannels implicated in a variety of inherited skin disorders.

Added value of this study

In this work, we administered the antibody to mutant mice that expressed pathological Cx30 hemichannels associated with Clouston syndrome and observed a reversal of the skin-related mouse phenotype within two weeks of treatment.

Implications of all the available evidence

These results suggest anti-Cx antibodies may develop effective therapies for Cx-related orphan diseases. We believe this study will pave the way to the use of similar antibodies for the treatment of other Cx-related pathologies.

In particular, no fewer than eleven genetic skin diseases have been linked to mutations in five Cx genes [2]. The protein products of Cx genes form hexameric structures known as "connexons" that may function as a regular plasma membrane channels, termed "hemichannels", or dock with other connexons from an opposing cell to self-assemble into gap junction intercellular channels [3]. In several instances, pathological conditions have been associated with more active or abnormally active Cx hemichannels, referred to also as "leaky" hemichannels [4,5].

Cx30 [6] is found at very low levels in interfollicular epidermis, but at high levels in nail beds, nail matrix and hair follicles [7]. Cx30 is upregulated during wound healing [8] and in patients with different hyperproliferative skin disorders [9]. Functional studies in expression systems reported an augmented activity for hemichannels comprising Cx30 p.A88V or Cx30 p.G11R [10], two pathological variants implicated in hidrotic ectodermal dysplasia [11], a human hereditary genodermatosis also known as Clouston syndrome [12-14]. When expressed in HeLa cells, both Cx30 p.G11R and Cx30 p. A88V variants formed abnormally active Cx hemichannels that promoted leakage of ATP from cell cytosol to extracellular medium, induced large voltage-activated currents and ultimately resulted in cell demise [10]. In both HeLa cells and rat epidermal keratinocytes (REK cells), expression of Cx30 p.A88V correlated with cell death due to potent activation of cleaved caspase-3 [15]. Likewise HaCaT cells, a human-derived keratinocyte cell line [16], became apoptotic via activation of caspase-3, -8, -9, and PARA following expression of Cx30 p. G11R or Cx30 p.A88V [17].

Maintenance of a healthy epidermal barrier [18] relies on a delicate balance between proliferation and differentiation [19], two cellular processes that are critically regulated by ionized calcium (Ca^{2+}) levels [20-22] and Cx expression [23,24]. ATP release in the epidermis [25-28] can activate Ca^{2+}-permeable P2X receptors and/or Ca^{2+}-mobilizing P2Y receptors on the surface of keratinocytes and other cells types [29,30]. Therefore, abnormal paracrine signaling due to ATP leakage though aberrant Cx hemichannels, such as Cx30 p.A88V hemichannels [10], has the potential to upset the delicate Ca^{2+}-dependent proliferation/differentiation balance in the epidermis and may lead to breakdown of epidermal integrity.[4,5,24] In line with this hypothesis, $Cx30^{A88V/A88V}$ knock in mice (expressing Cx30 p.A88V in the homozygous state) exhibited enlarged SGs due to an increased number of sebocytes per SG, together with hyperproliferation of epidermal keratinocytes, as well as of cells forming the outermost layer of SGs [31], which are mitotically active [32]. Recent work has highlighted also an atypical auditory phenotype and altered expression of cochlear gap junction channels in $Cx30^{A88V/A88V}$ mice [33,34].

The goal of this study was to assay the *in vivo* efficacy of a potent antagonist antibody targeting Cx hemichannels [35,36]. Monoclonal antibodies "have made a striking transformation from scientific tools to powerful human therapeutics" [37], and many are already on the market or under advanced clinical development [38]. In prior work, we first selected Cx-binding human antibody fragments by screening a vast library expressed in phage [35]. The selected fragments comprised a heavy chain variable domain (V_H, 122 amino acids, a.a.) and a light chain variable domain (V_L, 108 a.a.) connected by a 7 a.a. flexible spacer to create a single-chain fragment variable (scFv) complex, whose structure we solved by X-ray crystallography (Protein Data Bank accession code 5WYM). Next, we formed abEC1.1 by fusing the Cx-binding scFv with the hinge and fragment constant (Fc) domain of human immunoglobulin G1 (IgG1, see Materials and Methods) [35]. We generated also a chimeric version (abEC1.1m) with murine hinge and Fc domain [36]. Both scFv-Fc polypeptides (see Supplementary materials, Fig. S1, and Materials and Methods, section 2.1) formed homodimers with a MW of ~103 kDa through a diabody interaction between V_H and V_L [39] and disulfide bonds in the hinge region [40]. Patch clamp recordings showed the monoclonal antibodies so constructed inhibit equally well Cx26, Cx30 and Cx32 hemichannels, but are ineffective on pannexin 1 channels [36]. By performing *in silico* analysis of Cx hemichannel-antibody interaction, we identified critical amino acids (N54, T55, L56, Q57, P58, P175 and N176) that are conserved in the extracellular domain of Cx26, Cx30 and Cx32 [36]. Of note, even a single a.a. difference in the above a.a. list reduced drastically the inhibitory effects of the antibodies on all other tested Cx hemichannels (Cx30.2/31.3, Cx30.3, Cx31, Cx31.1, Cx37, Cx43 and Cx45) [36], most of which are expressed in the skin and its appendages [41-45].

Here, we extended the *in vitro* studies summarized above to include *in vivo* analyses based on the $Cx30^{A88V/A88V}$ mouse model of Clouston syndrome [31]. We report that two weeks of antibody treatment, either topical or systemic, are sufficient to counteract the effects of pathological Cx30 expression in the skin of these mutant mice. Altogether, our results suggest anti-Cx antibodies may develop effective therapies for Cx-related orphan diseases.

2. Materials and methods

2.1. Antibody generation

The gene encoding the Cx-binding scFv complex [35] was inserted into a cloning plasmid (Cat. No. pfuse-hg1fc2, Invivogen, Hong Kong) to generate a scFv-Fc fusion protein comprising constant hinge, CH_2 and CH_3 domains of human secreted IgG1 [46]. A similar cloning plasmid (Cat. No. pfuse-mg1fc2, Invivogen) was used to generate a chimeric version with constant hinge, CH_2 and CH_3 domains of mouse secreted IgG1 (see e.g. UniProtKB − P01868). For antibody production, a FreeStyle™ 293-F cell line (Cat. No. R79007, ThermoFisher Scientific, Waltham, MA, U.S.A.), maintained in Freestyle 293 Expression Medium (Cat. No. 12338026, ThermoFisher Scientific), was stably transfected with the expression vector of either scFv-Fc polypeptide. Cells were tested periodically with the MycoFluor™ Mycoplasma Detection Kit (Cat. No. M7006, ThermoFisher Scientific) to exclude contamination. Expressed antibodies were purified using HiTrap MabSelect™ columns (Cat. No. 28-4082-53, GE Healthcare, Pittsburgh, PA, USA) with the ÄKTApurifier 100 system (GE Healthcare) following the Manufacture's instruction. After purification, the buffer was exchanged to phosphate buffer saline (PBS, pH 7.4) and the antibodies were kept in PBS at 4°C [36].

2.2. Animals and genotyping

All animal experimentation was conducted in adherence to the NIH Guide for the Care and Use of Laboratory Animals and

recommendations from both ARRIVE and PREPARE guidelines [47,48]. In Italy, mice were bred and genotyped at the National Research Council-Institute of Biochemistry and Cell Biology (CNR-IBBC), Infrafrontier/ESFRI-European Mouse Mutant Archive (EMMA), Specific Pathogen-Free (SPF) barrier unit (Monterotondo Scalo, Rome). All the experimental procedures were agreed upon, reviewed and approved by local animals welfare oversight bodies and were performed with the approval and direct supervision of the CNR-IBBC/Infrafrontier—Animal Welfare and Ethical Review Body (AWERB), in accordance with general guidelines regarding animal experimentation, approved by the Italian Ministry of Health, in compliance with the Legislative Decree 26/2014 (ref. Project licenses N.68/2016-PR and 603/2018-PR), transposing the 2010/63/EU Directive on protection of animals used in research. In China, mice were bred and genotyped at Shanghai Biomodel Organism Science & Technology Development Co., Ltd., Shanghai (China), shortened as ShBio. All *in vivo* experiments for this work were performed at ShBio under animal production license sxck(Shanghai)2017-010 and animal usage license: sxck(Shanghai)2017-012. Experimental animals were culled by trained personnel using gaseous anesthesia followed by a rising concentration of CO_2 and cervical dislocation to confirm death, or cervical dislocation alone.

In Cx30$^{A88V/A88V}$ knock in mice [*mus musculus*, allelic composition: *Gjb6*$^{tm2.2Kwi}$/*Gjb6*$^{tm2.2Kwi}$; EMMA ID: 07626; Mouse Genome International Database (MGI) ID: 5607781], expression of the Cx30 p.A88V variant is controlled by the endogenous Cx30 promoter, and is also linked to the expression of a lacZ reporter gene that codes for ß-galactosidase, which can be used to monitor Cx30 p.A88V expression *in vivo* [31]. These mice, which were originally on a mixed CD1;129P2 background, were backcrossed to C57BL/6N and interbred in the heterozygous state (*Gjb6*$^{tm2.2Kwi/+}$). Both males and females were used for these studies: P2 pups to harvest primary keratinocytes; adult animals aged 6 to 8 weeks for all other studies.

For some control experiments, we used also Cx30 null mice (*mus musculus*, allelic composition: *Gjb6*^{tm1Kwi}/*Gjb6*^{tm1Kwi}; EMMA ID: 00323; MGI ID: 2447863), in which exon2, including the whole open reading frame of Cx30 (*Gjb6*), is homologously replaced by the open reading frame of LacZ. *Gjb6*$^{-/-}$ mice were backcrossed to C57BL/6J mice and interbred in the heterozygous state (*Gjb6*$^{+/-}$) for more than 10 generations. Both males and females were used, aged 6 to 8 weeks.

Genotyping protocols were performed by PCR on extracted mouse tail tips using the primers previously described. Specifically, for Cx30 p.A88V knock in mice (*Gjb6*$^{tm2.2Kwi}$/*Gjb6*$^{tm2.2Kwi}$) primer pairs were:

A88VF 5'−GGT CGA AGG AAC CTT TCA CAG G−3'
A88VR 5'−GCT ACC ATC ACG TGC TCT TTG G−3'

For Cx30 null mice (*Gjb6*^{tm1Kwi}/*Gjb6*^{tm1Kwi}) primer pairs were specific for the wt alleles:

Cx30F 5'−GGTACCTTCTACTAATTAGCTTGG−3',
Cx30R 5'−AGGTGGTACCCATTGTAGAGGAAG−3'.

To visualize the deletion, primers specific for the *lacZ* region (that flanks the deleted allele) were used in combination with the corresponding wt forward primer:

Cx30lac 5'−AGCGAGTAACAACCCGTCGGATTC−3'.

2.3. Study design

Mice were allocated to the different treatment groups by weight, gender, and littermate randomization. To minimize subjective bias, sample identity (e.g. genotypes) was randomized by associating an identification number to each sample before processing. In order to construct the optimal experimental design and estimate the minimum number of animals necessary for the experiments (sample size of the groups) for each type of experiment, and for each genetically modified and control strain, we set a probability $\alpha = 5\%$ for the type I error in the ANOVA test. Then, fixing $\beta = 4\alpha = 20\%$ so as to obtain a test power of $1 - \beta = 80\%$, we have calculated the number n of each of the two samples to be compared using the formula:

$$n = 2 \left[\frac{(z_{\alpha/2} + z_{\beta}) \cdot \sigma}{\Delta} \right]^2$$

with $z_{\alpha/2} = 1.96$ and $z_{\beta} = 1.28$. Based on experiments of the same type carried out with the used markers of cell proliferation and differentiation, we quantified the variability of the data (variance, σ^2) and established the minimum difference $\Delta = \mu_1 - \mu_2$ between averages that had a biological significance. No sample was excluded from the analysis.

2.4. Antibody administration

For systemic administration, antibodies with mouse Fc (abEC1.1m) were dissolved in PBS and dosed at either 5 mg or 10 mg per kg of body weight for intravenous and intraperitoneal delivery, respectively. For topical administration, antibodies with human Fc (abEC1.1) were incorporated in cetomacrogol base cream (50 μg / ml) [49,50]; cream ingredients: Aqua, Petrolatum, Paraffinum Liquidum, Cetyl Alcohol, Stearyl Alcohol, Ceteareth-20, Sodium Benzoate, Potassium Sorbate, Benzyl Alcohol, Disodium EDTA, Citric Acid (as per supplier-provided information at http://www.makeitlab.eu). Twenty four hours before the start of treatment, animals were depilated on the back under gaseous anesthesia (2% isoflurane). On the day of treatment, they were administered 100 μl of antibody cream under anesthesia (2% isoflurane), which required a light massage to allow the cream to be completely absorbed by the skin. To minimize the number of animals used for topical treatment, each mouse was given abEC1.1 cream on the left side and an inactive isotype antibody cream on the right side of the back (negative internal control).

2.5. Antibody PK analysis

Ninety-six-well transparent plates (ThermoFisher, Cat. No. 468667) suitable for enzyme linked immunosorbent assay (ELISA) [51] were filled with 100 μl per well of pepEC1.1 solution [35] (1 μg/well, diluted in PBS), for blood samples, or Goat Anti-Human IgG (H+L) antibody (Cat. No. 109006003, Jackson Immuno Research, Ely, Cambridgeshire, U.K.) at a concentration of 0.5 μg/ml in CBS buffer for skin supernatant samples, and incubated overnight at 4°C. After washing once with PBST buffer (0.05% TWEEN20 in PBS), wells were blocked with 200 μl per well of M-PBST (5% milk in PBST) and incubated for 1 h at 37°C. After discarding the blocking solution, a standard curve was constructed as follows. Purified antibody at the maximum concentration of 1 μg/ml in PBS buffer was diluted stepwise, by a 2^n factor in PBS, down to a minimum concentration of 2^{-7} μg/ml. Fifty (50) μl of each diluted abEC1.1 solution was added in triplicate and incubated for 1 h at 37°C, then washed six times with PBST buffer. After washout, each well received 50 μl solution containing goat anti-human or anti-mouse horseradish peroxidase-conjugated antibody (Cat. No. W4038 or W4028, Sigma-Aldrich/Merck, China) diluted in PBS buffer (dilution factor 1:5000). Plates were incubated for 1 h at 37°C and washed six times with PBST buffer. Finally, 50 μl of substrate ABTS solution (Cat. No. 11684302001, Roche, Shanghai, China) were added to each well and absorbance at 405 nm was read out immediately plate reader (Enspire, Perkin Elmer, Waltham, MA, U.S.A.). The relationship established between absorbance and the known antibody concentration provided the standard curve.

For antibody serum pharmacokinetics (PK) analysis, blood samples (100 μl) were withdrawn at the following post-intravenous injection time points: 15 min, 30 min, 1 h, 3 h, 8 h, 24 h, 48 h, 72 h, 144 h for abEC1.1 (human Fc) and 15 min, 30 min, 1 h, 3 h, 8 h, 16 h, 24 h, 48 h, 72 h, 144 h, 288 h for abEC1.1m (mouse Fc). Collected samples were transferred to 1.5 ml tubes (Cat. No. 05408129, Thermo-Fisher Scientific,) and placed in 37°C water bath for 1 hour then centrifuged 1800 rpm at 4°C for 10 min. The supernatant serum (about 50 μl /sample) was transferred to fresh 1.5 ml tubes and stored at −80°C. The amount of antibody in each serum sample was quantified according to absorbance at 405 nm and standard curve, after thawing and proper dilution in PBS.

To detect antibody in the skin, 100 μl of antibody cream was applied and massaged until visibly absorbed by the skin. Thereafter, mice were humanely euthanized at different time points, the skin was harvested, chopped and placed in lysis buffer (Cat. No. P0013B, Beyotime Biotechnology, China) containing protease inhibitor PMSF (Cat. No. ST506, Beyotime). Skin samples were homogenized and centrifuged (16000 g, 30 minutes, at 4°C), supernatant was transferred to fresh tubes and stored at −80°C. The amount of antibody in each skin sample was quantified by ELISA, according to absorbance at 405 nm, as described above for purified antibody samples.

2.6. Multiphoton confocal fluorescence imaging of sebaceous glands

Freshly excised skin samples comprising both epidermal and dermal layers were maintained in short term culture in a Trowell-type system, with dermal side immersed in DMEM/F12 (Cat. No. 11320-074, ThermoFisher Scientific) supplemented with 10 % FBS (Cat. No. 10270-106, ThermoFisher Scientific) and the *stratum corneum* of the epidermis exposed to air. Residual hair was removed by gently applying a hair removal cream to the *stratum corneum* for 2 min, carefully wiping cream off with dry cotton buds and rinsing the skin surface tree times with PBS. Thereafter, the tissue was stained by applying a 400 μl drop of Nile Red (Cat. No. 72485-100MG, Sigma-Aldrich/Merck), dissolved in methanol at a concentration of 1 mg/ml and incubated for 30 min at 37°C. After complete penetration of Nile Red, the surface was cleaned again using cotton buds imbibed with 70% ethanol, followed by tree more rinses with PBS. Samples maintained in the Trowell-type system were transferred to the stage of a custom-made multiphoton laser scanning confocal system based on the SP8 architecture (Leica Microsystems, Mannheim, Germany, EU) with stimulated emission depletion (STED) extension. The imaging system was equipped with a mode locked Ti:Sapphire multiphoton tunable laser source (wavelength range: 680-1080 nm; pulse width: 140 fs; Chameleon Vision II, Coherent Inc., Santa Clara, CA, USA) and wavelength extension (range: 1010-1340 nm; Chameleon MPX, Coherent). To excite Nile red fluorescence, the output of the Ti:Sapphire source at 840 nm was fed to the Chameleon MPX and the latter was tuned at 1080 nm. At this wavelength, the average power conveyed to sample through a 25 × water immersion objective (1.00 N.A., HC IRAPO L25 × /1.00 W motCORR, Leica Microsystems), was 20 mW. Images consisting of 1024 × 1024 pixels were acquired with a pixel resolution of 105 nm/pixel and pixel dwell time of about 100 μs from 20 consecutive focal planes at depth increments of 1.5 μm / step to form through-focus sequences (z-stacks) that were analyzed off-line using the public domain software ImageJ (https://imagej.nih.gov).

2.7. Confocal immunofluorescence analyses

Tissue biopsies were taken from the dorsal mid-thoracic region, fixed in 4% paraformaldehyde overnight at 4°C, dehydrated in increasing alcohol concentrations and embedded in paraffin. The 9 μm thick sections were stained with rat anti-Ki67 (monoclonal, diluted 1:50, Cat. no. M7249, DakoCytomation, Glostrup Denmark) according to the manufacturer's recommendations.

Skin biopsies were embedded in Killik embedding medium (Cat. No. 05-9801, Bio-Optica, Milan, Italy, EU) frozen and cryosectioned at a thickness of 12 μm using a CM 1950 cryostat (Leica Biosystems Nussloch GmbH, Nussloch, Germany). The cryosections were fixed in 100% ethanol at −20°C for 5 minutes, washed 3 times in TBS-TX (50 mM Tris,1,5% NaCl, 0,3% TritonX-100) and blocked for 1 h with 4% bovine albumin serum and 1% normal goat serum in TBS-TX. The primary antibody rabbit anti-Cx30 (Cat. no. 71-2200, ThermoFisher Scientific) was diluted (1:200) in blocking solution and incubated with cryosection over night at 4°C. After incubation, the sections were washed 3 times with TBS-TX and incubated for 45 min with fluorophore-conjugated secondary antibody Alexa Fluor 488 goat anti-rabbit IgG (diluted 1:500, Cat. no. A-11008, ThermoFisher Scientific). Sections were then washed twice with TBS-TX and nuclei were stained with $4',6-diamidino-2-phenylindole$ (DAPI, 1:1000, Cat. no. D1306, ThermoFisher Scientific) for 10 min. Actin filaments were stained with fluorescent phalloidin (Cat. No. A12380, ThermoFisher Scientific). All samples were mounted onto glass slides with a mounting medium (FluorSaveTM Reagent, Cat. No. 345789, Merk) and analyzed using a confocal microscope (TCS SP5, Leica Microsystems) equipped with an oil−immersion objective (40 × HCX PL APO 1.25 N. A., Leica Microsystems).

2.8. Patch Clamp electrical measurements in HeLa DH cells

The coding regions of the wt *homo sapiens* Cx30 gene was synthesized (by Shanghai Sangon Biological Engineering Technology & Services Co., Ltd., Shanghai, China) without stop codon and subcloned into a pcDNA3.1(+) mammalian expression vector (Cat. No. V79020, ThermoFisher Scientific) that had been previously modified for C-terminal fusion of Cx genes with Venus, a circularly permuted mutant of the yellow fluorescent protein (YFP). The Cx30 p.A88V mutant was generated by replacing the alanine in position 88 with a valine using the Mut Express II Fast Mutagenesis Kit V2 (Cat. No. C214, Vazyme Biotech, Nanjing, China).

HeLa DH cells (Cat. No. 96112022, Sigma-Aldrich/Merck), which express no connexins, were seeded onto round glass coverslip (Cat. No. FIS#12-542A, ThermoFisher Scientific) and maintained in Dulbecco's modified Eagle's medium (DMEM, Cat. No. 41965039, ThermoFisher Scientific) containing 10% (v/v) Gibco fetal bovine serum (FBS, Cat. No. 10270-106, ThermoFisher Scientific) and 1% penicillin/streptomycin (5000 U/ml; Cat. No. 15070-063, ThermoFisher Scientific). Cells were tested periodically with the MycoFluor™ Mycoplasma Detection Kit (Cat. No. M7006, ThermoFisher Scientific) to exclude contamination. Twenty four hours after plating, the Lipofectamine 3000 transfection reagent (Cat. No. L3000-015, ThermoFisher Scientific) was used to transiently transfect HeLa DH cells at 25-30% confluence with the expression vectors described above.

Patch pipettes were fabricated from glass capillaries (G85150T-4, Harvard Apparatus, Edenbridge, UK) using a double stage vertical puller (PP-830, Narishige, Tokyo, Japan) or horizontal laser-based puller (P-2000, Sutter Instruments, Novato, CA, USA) and filled with a potassium aspartate-based intracellular solution (ICS$_{KAsp}$) containing (in mM): 125 KAsp, 10 NaCl, 10 KCl, 1 MgCl$_2$, 10 HEPES, 1 CaCl$_2$ and 4 BAPTA tetrapotassium salt (pH 7.2, 311 mOsm) and filtered through 0.22-mm pores (Cat. No. SLGP033RB, Millipore/Merck).

Twenty four hours after transfection, glass coverslips with adherent cells were transferred to the stage of an upright fluorescence microscope (BX51, Olympus Corporation, Tokyo, Japan) equipped with differential interference contrast (DIC) optics. Cells were continuously superfused at 2 ml/min at 20−23°C with a sodium chloride-based extracellular solution (ECS$_{NaCl}$) containing a reduced (0.2 mM) Ca^{2+} concentration ([Ca^{2+}]$_e$) and (in mM): 140 NaCl, 5 KCl, 10 HEPES, 2 sodium pyruvate, 4 tetraethylammonium chloride (TEA-Cl), 1 MgCl$_2$, 4 CsCl and 5 glucose (pH 7.4, 323 mOsm). Filled patch pipettes had resistances of 4-6 MΩ when immersed in ECS$_{NaCl}$. EGTA was

purchased from BBI, all other components for intracellular and extra-cellular solutions were purchased from Sigma-Aldrich/Merck.

Hemichannel currents were assayed in ECS_{NaCl} while keeping cells at -25 mV under whole cell patch clamp recording conditions. To promote hemichannel opening, cells were transiently depolarized to $+15$ mV for 6.2 s followed by a switch to -60 mV to elicit tail currents. Cells were held at this negative potential for 18.6 s before returning to -25 mV. To minimize stress to the plasma membrane, steps were replaced by voltage ramps lasting 20 ms. To estimate plasma membrane leak currents, Cx hemichannels were blocked by adding either 2 mM $CaCl_2$ or 50 μM flufenamic acid (FFA, Cat. No. F9005, Sigma-Aldrich/Merck) to the superfusion medium [35,52]. For antibody application, the opening of a glass micropipette connected to a pneumatic pico-pump (PV820, World Precision Instruments Inc., Sarasota, FL, USA) and filled with the ECS_{NaCl} extracellular solution supplemented with abEC1.1 (952 nM) was positioned near the patched cell. During antibody delivery, the superfusion was stopped.

2.9. Isolation and culture of primary mouse keratinocytes

Primary keratinocytes (KCs) were harvested from P2 pups of either genotype (mutant and their wt littermates) sacrificed by decapitation using scissors, thereafter limbs and tail were cut off [53]. To peel off the whole skin, sharp scissors were inserted through the hole at the tail and skin was cut along the dorsal midline of the body to the opening on the neck. Next, one forceps was used to grasp the exposed body and another forceps to grasp the skin, and gently peel the whole skin off the body and over the leg stumps with one continuous motion. The skin thus peeled off as one intact piece was rinsed with 15 mL of sterile PBS in a 10 cm Petri dish. The skin from each pup was transferred into a 2 mL tube filled with ice cold dispase digestion buffer, which contains 4 mg/mL dispase dissolved in KC growth medium (Cat. No. MEPICF500, ThermoFisher Scientific) supplemented with 0.06 mM $CaCl_2$, dGS (Cat. No. S0125, ThermoFisher Scientific), and antibiotics/antimycotics. Incubation in dispase was carried out overnight in a 4°C refrigerator on a rotator, making sure that the skin was not folded in the tube as this would result in insufficient exposure of the folded region to the dispase solution. After 12-18 h in dispase, each skin samples was transferred, together with the dispase solution, to a new Petri dish with 15 mL sterile PBS to wash away excess dispase. Using two pairs of forceps, the skin was grasped from PBS, lifted and transferred to a new Petri dish with the epidermal side down and the dermis side up. Carefully stretching the skin folds ensured that it was fully extended on the Petri dish. For each skin sample, 500 μL of Trypsin-EDTA 0,25% (Cat. No. 25200056, ThermoFisher Scientific) were placed in a new Petri dish. Using forceps, the dermis was slowly lifted up and away from the epidermis, while holding the epidermis down. The separated epidermis was transferred and floated on each drop of trypsin solution with the basal layer downward to ensure efficient digestion of basal KCs from the epithelium. Incubation in the trypsin solution was carried out at room temperature (with the lid covered) on a horizontal shaker with gentle agitation for 20 min. Thereafter, 2 mL of supplemented KC growth medium per epidermis (about 1 square inch in size per epidermis) were added to the Petri dish. The epidermis was grasped using forceps, and vigorously rubbed back and forth to release single cells from the epidermal sheet, signaled by the medium turning increasingly turbid as cells are detached from the epidermis. The Petri dish was tilted to collect and transfer the cell suspension to a new tube, leaving the remaining epidermal sheet on the dish. To maximize the yield, this procedure was repeated two more times after adding 2 mL KC growth medium. Cell suspensions were combined in the same tube, pipetted up-and-down gently a few times to break any cell clumps using the appropriate serological pipettes, then passed through a 100 μm filter to a new 50 mL centrifuge tube. The filtered cells were centrifuged for 5 min at 180 g. The supernatant

was aspirate off and the cell pellet was gently resuspended in 1 mL cold KC growth medium/epidermis. The cells were counted using an automated cell counter (Countess™ Automated Cell Counter, Cat. No. C10227, ThermoFisher Scientific) and seeded at a density of 5×10^4/ cm^2 in KC growth medium in culture dishes pre-coated with collagen (Cat. No. A1048301, ThermoFisher Scientific) to promote cell adhesion. Cells were cultured in humidified incubator with 5% CO_2 at 37° C. To remove unattached cells, the medium was changed 24 h after the initial plating the medium. Thereafter, it was changed every 48 hours until the cells reach the desired confluence level prior to the experiment (generally 3 to 7 days).

2.10. Patch clamp recordings and Ca^{2+} imaging in primary mouse keratinocytes

KCs, isolated and cultured as described above, were continuously superfused at 2 ml/min and 20$-$23°C with a solution containing either 60 μM $CaCl_2$ or 2 mM $CaCl_2$ and (in mM): 140 NaCl, 5 KCl, 10 HEPES, 2 Sodium Pyruvate, 5 Glucose, 1 $MgCl_2$ (pH 7.3, 323 mOsm). Patch pipettes were filled with a cesium chloride-based intracellular solution (ICS_{CsCl}) containing (in mM): 140 CsCl, 10 HEPES, 0.3 EGTA (pH 7.2, 311 mOsm) and filtered through 0.22-mm pores (Millipore); antibody was applied for 15 min through the opening of a glass micropipette positioned near the patched cell, connected to a pneumatic pico-pump (PV820, World Precision Instruments Inc., Sarasota, FL, USA) and filled with the low Ca^{2+} extracellular solution supplemented with abEC1.1 (952 nM). For Ca2+ imaging, the pipette solution was supplemented with 50 μM Fluo-4 and EGTA was omitted. To test the effect of the antibody, keratinocytes were patch clamped after incubation for 30 min in the low Ca^{2+} extracellular medium supplemented with abEC1.1 (400 nM).

2.11. ATP release assay

HaCaT cells (Cat. No. 300493, Cell Lines Service GmbH) were cultured in petri dishes of 35 mm diameter as previously described [35] and tested periodically with the MycoFluor™ Mycoplasma Detection Kit (Cat. No. M7006, ThermoFisher Scientific) to exclude contamination. Cells grown to 30% of confluence were infected with a lentivirus engineered in the lab to express either human wt Cx30 or human Cx30 p.A88V using the pUltra-hot vector for bi-cistronic expression of mCherry and the gene of interest under the ubiquitin C promoter (Addgene plasmid # 24130, a gift from Malcolm Moore). Infected cells were plated at a density of 5×10^4 cells/cm^2 onto round glass coverslips (Cat. No. 1051201, Heinz Herenz, Hamburg, Germany) 24 hours before the experiment. On the day of the experiment, each glass coverslip was transferred into a 24-well plate, complete DMEM was removed, cells were washed twice with serum-free DMEM and incubated for 30 minutes at 37°C and 5% CO_2.

ATP release was tested in 4 different conditions, depending on the solution used. To initiate the ATP release measurement, cells were washed with NCS, containing a normal (1.8 mM) Ca^{2+} concentration and (in mM): 137 NaCl, 5.36 KCl, 0.81 MgSO4, 0.44 KH2PO4, 0.18 Na2HPO4, 25 HEPES and 5.55 Glucose (pH7.3), and incubated in NCS for 20 minutes at 37°C. The supernatant solution of each well of the 24-well plate was collected and kept on ice until ATP quantification. The same procedure was followed by incubating the same cells for 20 minutes at 37°C in ZCS, containing nominally zero calcium concentration and (in mM): 137 NaCl, 5.36 KCl, 0.44 KH2PO4, 0.18 Na2HPO4, 0.1 EGTA, 25 HEPES and 5.55 Glucose (pH7.3). Finally, after collecting the supernatant, the abEC1.1 antibody or FFA [35,52] were added to some of the wells to a final concentration of 400 nM or 50 μM respectively, and cells were incubated in these conditions for 40 minutes. To minimize ATP hydrolysis, each solution was supplemented with 100 μM ARL67156 (Cat. No. A265-5MG, Sigma-Aldrich/ Merck), an ectonucleotidase inhibitor [54]. The amount of ATP

released into each well of the 24-well plate during the 20 min incubation period in each condition was measured by transferring 25 μl of supernatant to a corresponding empty well of a black 96-well plate kept on ice. ATP was quantified using a luminometer (Victor Light 1420, Perkin Elmer) in conjunction with a bioluminescent ATP assay according to the Manufacturer's instructions (kit A22066, Thermo-Fisher Scientific). ATP standard curves were generated using serially-diluted concentrations of ATP and were used to convert measurements of luminescence signals into ATP concentrations. Experiments were performed in triplicate for each condition.

2.12. Statistics

Normality of distribution was ensured using the Kolmogorov−Smirnov test, and statistical comparisons of means were made by ANOVA and post-hoc comparison by Tuckey's test using *MATLAB* (R2019a, The MathWorks, Inc.). Mean values are quoted ± standard error of the mean (s.e.m.) unless noted otherwise. P = p-values < 0.05 indicate statistical significance.

3. Results

3.1. abEC1.1 inhibits Cx30 p.A88V hemichannels in vitro with IC$_{50}$ of 27 nM

The amino acid involved in the p.A88V mutation is located on the second transmembrane helix of Cx30 (Fig. 1a,b), at considerable distance from Cx extracellular domain that binds the scFv complex of the antibody [35,36] (see Materials and methods, section 2.1). Therefore we reasoned that the antibody might also interfere with the function of aberrant Cx30 p.A88V hemichannels. To test this hypothesis, we transiently transfected Cx-deficient HeLa DH cells with cDNA encoding Cx30 p.A88V and measured hemichannel currents in low (0.2 mM) extracellular Ca^{2+} conditions that favor the opening of a variety of different Cx hemichannels [55] (Fig. 1c). For these experiments, abEC1.1 was applied by pressure for 15 min through the
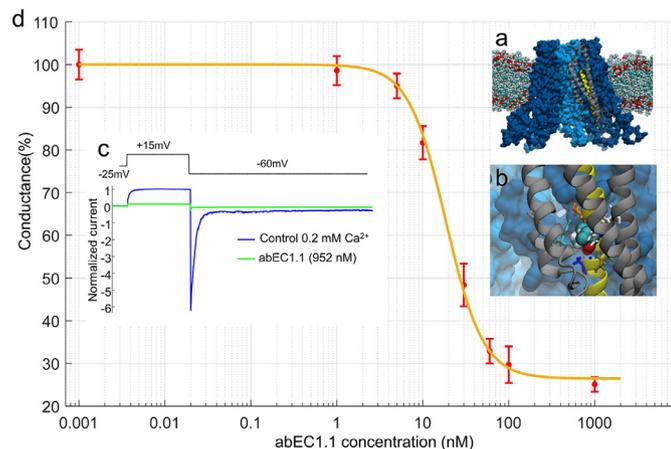
Fig. 1. The abEC1.1 antibody inhibits Cx30A88V hemichannel currents with IC$_{50}$ of 27 nM. **a**, Molecular model of a Cx30 hemichannel where alanine 88 has been replaced by a valine (A88V mutation). **b**, Magnified view of the V88 chemical environment. Proximal residues are shown with a licorice representation. **c**, Representative whole cell currents elicited by shown voltage commands (top, black trace); data were normalized to the mean value of the control response during the application of the +40 mV depolarization step; mean (thick traces) ± s.e.m. (thin traces) for n=5 cells before (blue traces, control) and after application of abEC1.1 at 952 nM for 15 min (green traces) in 0.2 mM Ca^{2+}. **d**, Percent membrane conductance (mean ± s.e.m. for n ≥ 5 cells), measured with the step protocol shown in panel **c** and normalized to pre-antibody application levels, vs. abEC1.1 concentration (see Materials and Methods, sections 2.1 and 2.8); the solid line is a least-square fit with a modified Hill equation $y = \alpha$ $[1+ (x/ \gamma)^2]^{-1} + \beta$, where x is antibody concentration (in nM), $\alpha = 73.5$, $\beta = (100 - \alpha) = 26.5$ and $\gamma = 18.61$ nM.

opening of a glass microcapillary placed in the proximity of the patched cell (see Materials and Methods, section 2.8). The dose-inhibition response curve of membrane conductance (normalized to pre-antibody application conductance) vs. abEC1.1 concentration (Fig. 1d, n ≥ 3 cells for each concentration) yielded IC$_{50}$ = 27 ± 5 nM (mean ± standard error of the estimate, S) [56]. The inhibitory effect of abEC1.1 on Cx30 p.A88V hemichannels was incomplete, leaving a 26% ± 6% (mean ± S) residual conductance at saturating concentrations (> 140 nM).

3.2. Assessment of antibody levels after single-dose administration to C57BL/6N mice

Assaying the pharmacokinetics (PK) of stable monoclonal antibodies is essential for designing efficacy and toxicity studies, as well as for optimizing dose and regimen in order to minimize risks and maximize the likelihood of success in subsequent clinical trials [57]. To obtain PK profiles (see Materials and Methods, sections 2.4 and 2.5), we performed single-dose systemic administration of abEC1.1 or abEC1.1m dissolved in PBS (5 mg of antibody per kg of mouse weight) via caudal vein injection to C57BL/6N mice, the genetic background of the Cx30$^{A88V/A88V}$ mutants used in this study (see Materials and Methods, sections 2.2 and 2.3). Thereafter, antibody serum levels were quantified by ELISA [51] (see Materials and Methods, section 2.5) at selected time points (Fig. 2a, n=3 mice per time point). Fitting antibody serum level vs. time with a double exponential function revealed a rapid distribution phase, with time constant τ_1, followed by a slower elimination phase, with time constant τ_2. The latter was approximately 3-fold longer for abEC1.1m (τ_2 = 127 hours = 5.3 days) compared to abEC1.1 (τ_2 = 43 hours = 1.8 days). In contrast, serum levels of abEC1.1m remained >140 nM for >136 hours = 5.5 days. The simplest explanation is that the human Fc of abEC1.1 promoted the formation of anti-therapeutic antibodies (ATA) which accelerated the disappearance of abEC1.1 from mouse serum [58]. Antibody serum levels (measured by ELISA) remained stable in excess of 200 nM for at least 4 days after a single intraperitoneal injection (100 μl) of abEC1.1m dissolved in PBS (10 mg of antibody per kg mouse body weight; Fig. 2b, n=3 mice per time point). Finally, we dispersed abEC1.1 in a cetomacrogol base cream and administered a single dose of abEC1.1 cream (100 μl containing 50 μg / ml of antibody) by light massage to the shaved back of the mice until completely absorbed in the skin [49,50]. Thereafter, antibody levels in the skin were quantified by ELISA on skin samples harvested at different time points, up to 24 hours post-administration. Fitting antibody level vs. time with a single exponential function yielded a time constant τ = 7.4 hours (Fig. 2c, n = 3 mice per time point).

3.3. Effects of antibody administration to live in mice

To quantify the most salient phenotypic trait of Cx30$^{A88V/A88V}$ mutant mice (see Materials and methods, section 2.2), i.e. their enlarged SGs [31], we acquired through-focus multiphoton confocal image sequences (z-stacks) in freshly excised back skin samples stained with Nile red (Supplementary materials, Fig. S2 and Fig. S3), a marker for intracellular lipids [31,59] (see Materials and methods, section 2.6). In untreated Cx30$^{A88V/A88V}$ mice, we found a 1.6-fold larger number of sebocytes per SG (N_s) compared to wt controls, i.e. untreated Cx30$^{+/+}$ littermates with normal *Gjb6* alleles (N_s = 21.2 ± 0.7, mean ± s.e.m., n = 6 untreated mutants; N_s = 13.2 ± 0.7, n = 6 untreated wt mice; P = 1.3 × 10^{-5}, ANOVA).

Based on the results of Fig. 2c, we decided to treat mutant mice topically with daily applications of abEC1.1 cream (100 μl, containing 50 μg / ml of antibody; see Materials and Methods, section 2.4). In a separate group of mice, we also tested the effect of intraperitoneal injection with abEC1.1m (100 μl, 10 mg of antibody per kg of mouse weight; repeated at 3 days intervals based on the results of Fig. 2b).

The following is an account of the results achieved at the end of two weeks of treatment (Fig. 3).

The N_s count in back skin samples of mutant mice treated with abEC1.1 cream was reduced to wt levels (N_s = 14.4 ± 0.4, n = 8 treated mutants; P = 4.6 × 10^{-7} vs. n = 6 untreated mutants; P=0.143 vs. n = 6 untreated wt controls; ANOVA). Treatment with a cream formulation containing an inactive isotype control antibody had no effect (N_s = 22.9 ± 0.9, n = 4 treated mutants; P = 0.212 vs. n = 6 untreated mutants; P=9.6 × 10^{-7} vs. mutants treated with abEC1.1; ANOVA). Systemic treatment of with abEC1.1m was as effective as topical treatment with abEC1.1 cream (N_s = 13.4 ± 0.3, n = 7 mutants treated with abEC1.1m; P = 4.6 × 10^{-7} vs. n = 6 untreated mutants; P = 0.865 vs. n = 6 untreated wt; P = 0.063 vs. n = 8 mutants treated with abEC1.1 cream; ANOVA). None of above mentioned treatments had any effect on the N_s of wt mice (P > 0.5 vs. n = 6 untreated wt). These results are summarized graphically in Fig. 3a, b. To confirm expression of the antibody target in mouse sebocytes, we performed also an immunofluorescence assay with a commercial antibody that binds an intracellular epitope of Cx30 not affected by the p.A88V mutation (Fig. 3c; see Materials and Methods, section 2.7).

The Ki-67 proliferation marker [60] is expressed in epidermal keratinocytes as well as in cells of the outermost layer of SGs [31], which are mitotically active [32]. As shown in Fig. 4, Ki-67 immunoreactivity in back skin samples of untreated mutant mice (see Materials and Methods, section 2.7) was 5-fold higher compared to untreated wt littermates (n = 3 mice of each genotype, P = 7.3 × 10^{-5}; ANOVA). Treatment with abEC1.1 cream reduced Ki-67 immunoreactivity by 52 % ± 16 % (n=2 mutant mice; P = 0.010; ANOVA), whereas the inactive isotype antibody failed to produce measurable changes (n=2 mutant mice; P = 0.559; ANOVA).

Summarizing, these *in vivo* results indicate that both topical treatment with abEC1.1 and systemic treatment with abEC1.1m achieved a remarkable anti-proliferative action in the skin and reduced SG hypertrophy, the most salient phenotypic trait of these mutant mice.

3.4. abEC1.1 reduces Ca^{2+} influx and ATP release through mutant Cx30 hemichannels

As noted above, genodermatoses linked to hyperactive Cx hemichannels may share a common pathogenetic mechanism due to abnormal hemichannel-mediated ATP leakage and associated epidermal Ca^{2+} signaling deregulation [4,5,10]. To determine whether antibody action may impact on these key pathways, we performed patch clamp recordings in primary epidermal keratinocytes isolated from mutant mice (see Materials and Methods, sections 2.9 and 2.10). As shown in Fig. 5a, 2 mM extracellular Ca^{2+}, which blocks Cx30 wt hemichannels [61], blocked only partially hemichannel currents of mutant keratinocytes at negative membrane potentials, and was completely ineffective at positive membrane potentials. In contrast, abEC1.1 (952 nM) exerted an inhibitory effect on the whole cell currents of these keratinocytes at both negative and positive potentials (Fig. 5a).

by a double exponential function $f(t) = A_1 \exp(-t/\tau_1) + A_2 \exp(-t/\tau_2)$ where the coefficients (with 95% confidence bounds) are: A_1 = 675 nM (607, 743), τ_1 = 1.4 h (1.1, 2.0), A_2 = 132 nM (77, 187), τ_2 = 43 h (24, 213) for abEC1.1; A_1 = 291 nM (230, 352), τ_1 = 9.5 h (6.8, 16.1), A_2 = 402 nM (338, 466), τ_2 = 127 h (101, 171) for abEC1.1m. Intersection of the red dashed lines determines the time (136 h) at which the blood concentration of abEC1.1m falls below 140 nM. **b**, Measurement of abEC1.1m concentration in serum by ELISA vs. time following intraperitoneal injection at time t = 0 (10 mg of antibody per kg mouse body weight). **c**, estimate of antibody concentration in skin protein extract by ELISA following topical administration of antibody dispersed in cetomacrogol cream (50 μg / ml);[49] a single application of 100 μl of cream was massaged until completely absorbed in the depilated skin of the mouse back. Data (absorbance at 405 nm; arbitrary units, A.U.) were fitted by an exponential function $f(t) = A \exp(-t/\tau)$ where the coefficients (with 95% confidence bounds) are: A = 0.71 (0.62, 0.80), τ = 7.2 h (5.9, 10.2), hence $t_{1/2}$ = ln(2) τ = 5.1 h (4.1, 7.1).

Fig. 2. Antibody levels in serum and skin following single dose administration to C57BL/6N mice. All experiments related to this figure were performed on mice aged 6 to 8 weeks, n = 3 mice per time point (see Materials and Methods, sections 2.4 and 2.5). **a**, Measurement of abEC1.1 (black) and abEC1.1m (blue) concentration in serum by ELISA vs. time following intravenous bolus injection (100 μl) into the caudal vein at time t = 0 (5 mg of antibody per kg of mouse weight, 5 mg / kg). Each data set was fitted

Fig. 3. Effect of antibody treatment on sebaceous glands. All experiments related to this figure were performed on mice aged 6 to 8 weeks (see Materials and Methods, sections 2.2, 2.3, 2.4 and 2.6). **a**, Counting of Nile red positive cells in sebaceous glands (N_s) of in freshly explanted back skin samples from mutant mice and their wild-type littermates treated topically with abEC1.1 or an inactive isotype antibody, or treated systemically with abEC1.1m; results for non-treated controls are also shown. Legend: n = number of mice; m = number of sebaceous glands; P = p-value (ANOVA). **b**, Representative multiphoton confocal fluorescence images of Nile red stained sebocytes. Scale bar: 20 μm (see also Supplementary materials, Fig.S2 and Fig. S3). **c**, Cx30 immunoreactivity in sebaceous glands (asterisks); shown are maximal projection renderings of 10 consecutive confocal optical sections taken at 1 μm intervals; actin filaments were stained with fluorescent phalloidin (red); the green signal is due to a fluorophore-conjugated secondary antibody; in the epidermis and distal end of the hair follicle, the green signal was due to non-specific binding of the secondary antibody, as shown by its persistence in section from Cx30 knock out mice. Scale bar: 20 μm.

a

b
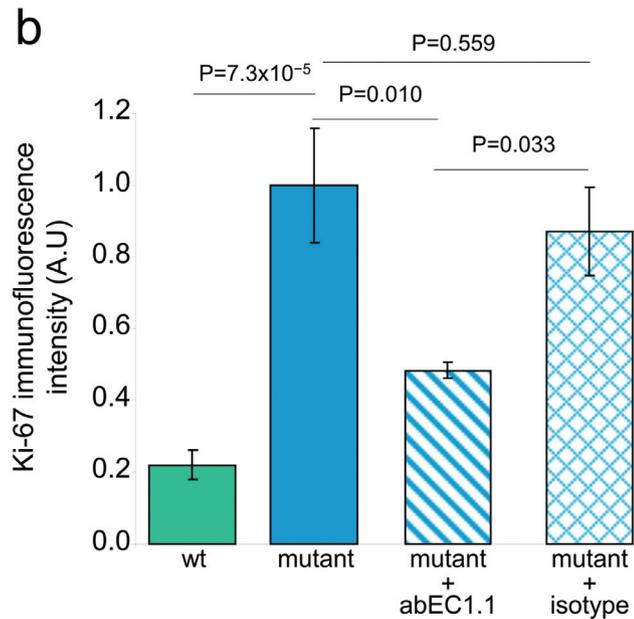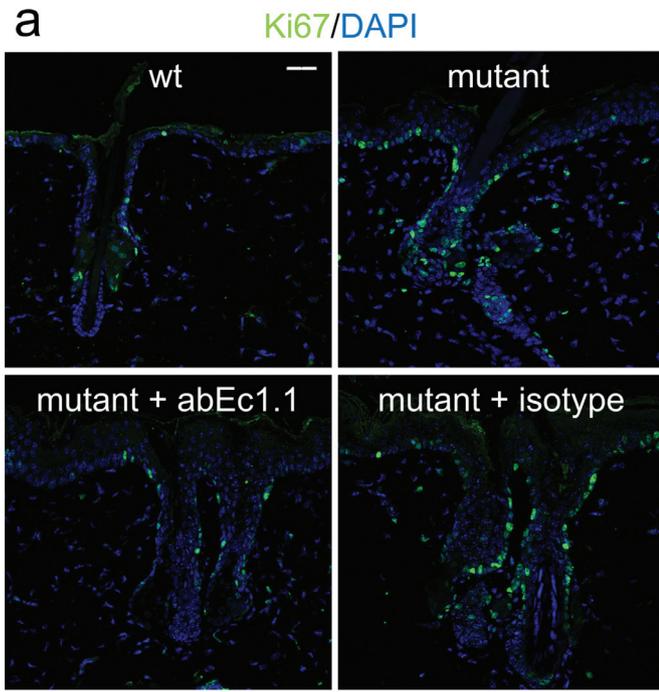
Fig. 4. Effect of antibody treatment on the expression of the Ki-67 proliferation marker. All experiments related to this figure were performed on mice aged 6 to 8 weeks (see Materials and Methods, section 2.7). **a**, Representative transversal sections of mouse dorsal skin showing cells that line the envelope of sebaceous glands labeled with an antibody that binds Ki-67 proteins (green). Shown are maximal projection renderings of nine consecutive confocal optical sections taken at 1.0 μm intervals; scale bar: 30 μm. **b**, Ki-67 immunoreactivity data (mean $\pm$ s.e.m.) obtained by analyzing 7 microscopic fields of view, each field=323 $\times$ 323 μm^2, from n=3 non-treated mice (wt and mutant littermates) and n=2 treated mice (mutant+abEC1.1 cream, or mutant + isotype antibody cream); P = p-value (ANOVA).

Based on these results, we predicted that mutant keratinocytes should import more Ca^{2+} than wt keratinocytes at negative membrane potentials. To test this hypothesis, we combined patch clamp recordings with Ca^{2+} imaging in isolated keratinocytes loaded with Fluo-4 (Fig. 5b). At -40 mV, Fluo-4 fluorescence emission (F) fractional changes ($\Delta F/F_0$) were 4.6-fold larger (P = 1.2 $\times$ 10^{-3}) in mutant keratinocytes (32% $\pm$ 2.7%, n=5 cells) compared to wt controls (6.9%

a

b

c
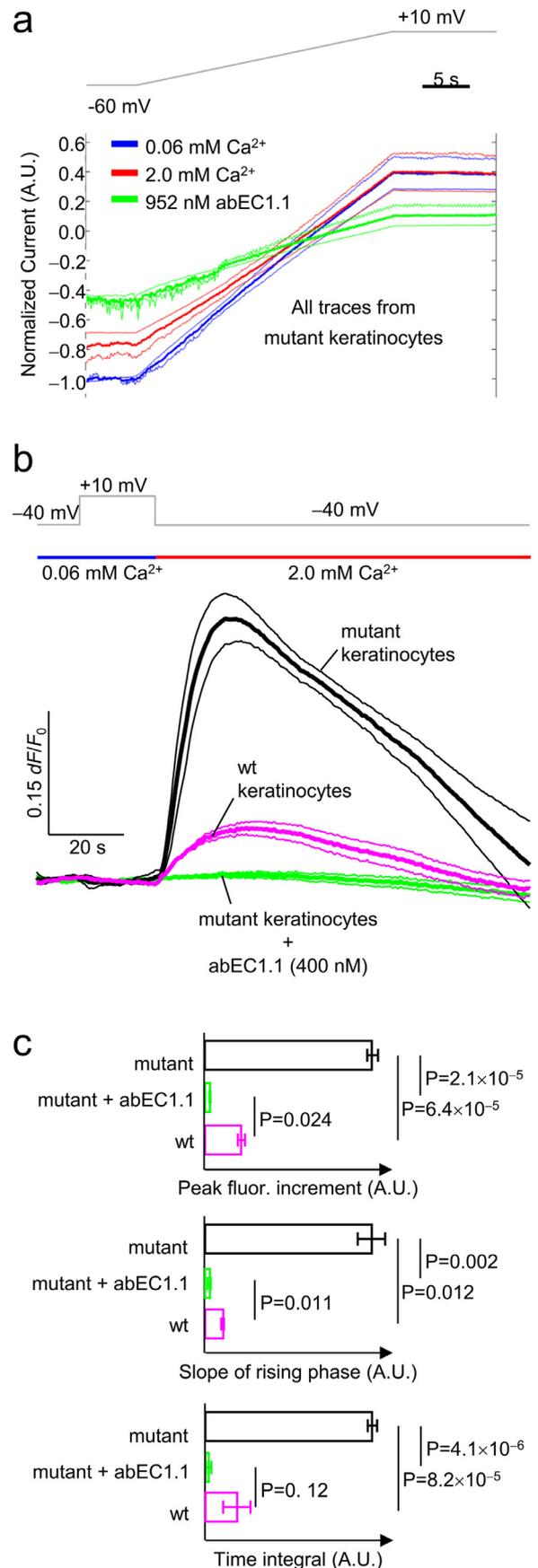
Fig. 5. Effect of acute antibody application on mouse isolated primary keratinocytes. All patch clamp and Ca^{2+} imaging experiments related to this figure were performed on primary keratinocytes isolated from P2 pups (mutant mice and age-matched wt
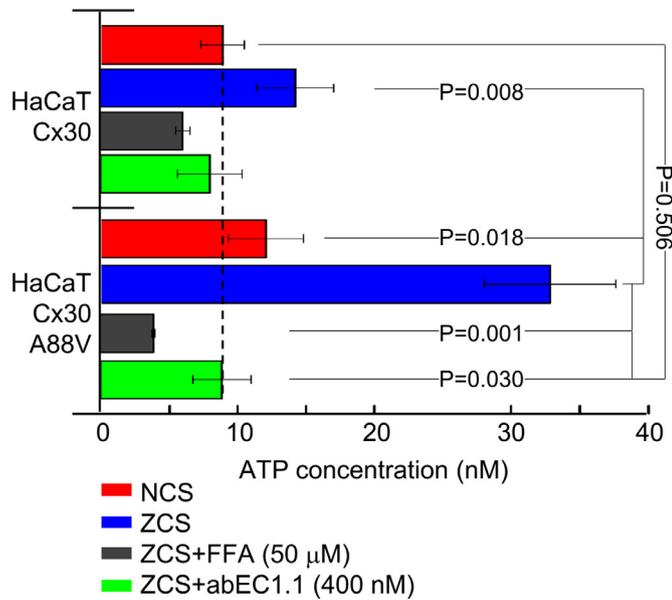
Fig. 6. Effect of acute antibody application on ATP release in cultured HaCaT cells. All experiments related to this figure were performed in HaCaT cells infected with a lentivirus expressing either human wt Cx30 or human Cx30A88V (see Materials and Methods, section 2.11). NCS, extracellular medium containing a normal 1.8 mM $[Ca^{2+}]_e$; ZCS, extracellular medium containing zero $[Ca^{2+}]_e$; FFA, flufenamic acid. Shown are ATP concentration in the supernatant (mean ± s.e.m.) for n = 3 independent experiments in each of the 4 conditions tested (4 to 12 different cultures in each condition): NCS, ZCS, ZCS + FFA (50 μM) and ZCS + abEC1.1 (400 nM); P=p-values (ANOVA).

± 1.8%, n=5 cells). Incubating mutant keratinocytes for 20 min with abEC1.1 (400 nM) abrogated the Ca^{2+} influx responsible for these fluorescence increments (for statistical data analysis, see Fig. 5c).

In a final set of experiments (Fig. 6), we measured ATP release in cultures of HaCaT cells (see Materials and Methods, section 2.11), a human skin-derived keratinocyte cell line [16]. HaCaT cells expressing Cx30 p.A88V released 2 times more ATP then those expressing wt Cx30 (P=0.009) when bathed in a zero Ca^{2+} solution (ZCS), consistent with prior results in HeLa transfectants [10]. Supplementing the ZCS with 400 nM abEC1.1 reduced this augmented ATP release to a level indistinguishable from that of HaCaT cells expressing wt Cx30 and bathed in 2 mM Ca^{2+} solution (NCS, P = 0.506). We observed a significantly reduced ATP release (P = 0.001) also following incubation of HaCaT cells expressing Cx30 p.A88V in the ZCS supplemented with FFA (50 μM), a non-specific blocker which can discriminate Cx hemichannels from pannexin channels in cellular ATP release [52]. Together, these results suggest that the effects observed *in vivo* after abEC1.1 administration may ensue from antibody-dependent

littermates; see Materials and Methods, sections 2.2, 2.9 and 2.10). **a,** Hemichannel currents recordings. Voltage ramps (gray trace, top) were applied to the same cell first in 60 μM extracellular Ca^{2+} concentration ($[Ca^{2+}]_e$) (blue traces), then in 2 mM $[Ca^{2+}]_e$ (red traces) or 60 μM $[Ca^{2+}]_e$ plus 952 nM $[abEC1.1]_e$ (green traces). Currents from each cells were normalized to the level recorded at the -60 mV pre-ramp holding potential in 60 μM $[Ca^{2+}]_e$ conditions. Shown are mean values of normalized currents (thick lines) encompassed in 95% confidence intervals (thin lines) for n=3 keratinocytes. **b,** simultaneous patch clamp and Ca^{2+} imaging. Top gray trace: voltage clamp protocol; one second before stepping down from +10 mV to -40 mV in 0.06 mM $[Ca^{2+}]_e$ (blue horizontal bar) a solution containing 2 mM $[Ca^{2+}]_e$ was applied by pressure through a micropipette positioned in the proximity of the patched cells (red horizontal bar). This procedure elicited measurable Fluo-4 signals both in wt keratinocytes (purple traces) and mutant keratinocytes (black traces). In the latter, Fluo-4 signals were abolished by the antibody (green traces). Shown are mean values (thick lines) ± s.e.m. (thin lines) for n=4 wt and n=5 mutant keratinocytes. **c,** Statistical analysis of the results in panel **b**. The slope of the rising phase was measured by fitting a straight line to the first 10 s seconds of each fluorescence trace in 2 mM $[Ca^{2+}]_e$ conditions at -40 mV; the time integral was measured over the entire trace segment in 2 mM $[Ca^{2+}]_e$ conditions at -40 mV. P = p-value (ANOVA).

reduction of abnormal Ca^{2+} entry and reduction of ATP release through hyperactive Cx30 p.A88V hemichannels.

4. Discussion

The etiopathogenesis of diseases linked to Cx mutations remains largely unknown [1]. However, a substantial body of data support the notion that the subset of pathologies linked to leaky Cx hemichannels may be caused by unregulated flux of key signaling molecules, such as Ca^{2+} and ATP, in and out of the cell [4,5]. Ca^{2+} may activate intracellular pathways whereas ATP released from the cell can act as a paracrine or autocrine signal [4]. In the skin, deregulated paracrine signaling due to extracellular ATP has the potential to compromise Ca^{2+}-dependent proliferation/differentiation balance, hence epidermal integrity [4,5,10]. It has long been known that the Ca^{2+} binding proteins calmodulin [62] and centrin-2 [63] are required for mitosis. More recent studies demonstrated that chromosome condensation is influenced by Ca^{2+} [64]. In addition, spatial restriction of a genetically encoded Ca^{2+} sensor detected a focally restricted centrosome-based Ca^{2+} signal in mitotic cells [65]. These findings are helping to clarify the crucial yet incompletely defined link between Ca^{2+} signaling, cell cycle progression, arrest and apoptosis [66].

The patch clamp results presented in this article confirm abEC1.1 can block Ca^{2+} influx into primary epidermal keratinocytes expressing pathological mutant hemichannels. In addition, our assays in HaCaT cells suggest the antibody may also contribute to diminish ATP release through leaky hemichannels. Together, these actions may gain control over leaky hemichannels and contribute to restoring rapidly epidermal homeostasis (Fig. 7).

Pannexin 1 channels (Panx1) are thought to mediate ATP release in different cellular systems [67-70], however we have already shown the abEC1.1 antibody is inactive on Panx1 [36]. In addition, (i) what we measured was the variation of ATP release caused by zeroing the extracellular Ca^{2+} concentration, a maneuver that enhances the open probability of Cx hemichannels formed by a variety of different Cxs [55], whereas pannexin channels are not directly gated by extracellular calcium [71]; (ii) FFA, used here at a concentration of 50 μM to inhibit ATP release, showed only modest inhibition of Panx1 at 300 μM [52].

Regulating cell physiology through the modulation of specific cellular channels represents a new iteration for the use of antibodies. In particular, taming the activity of more active or hyperactive hemichannels using antibodies that target extracellular Cx domain may enforce an entirely new therapeutic strategy. Indeed, as shown here, two weeks of antibody treatment sufficed to reduce hyperproliferation of sebaceous glands in the only available mouse model of Clouston syndrome, with no detectable side effects. We obtained comparable results both with systemic and with topical antibody application. As for the latter, neutralizing antibodies incorporated into the same cream vehicle used here, and applied topically to the skin in a murine model of epidermolysis bullosa acquisita, penetrated into the basal epidermis and upper papillary dermis reducing the severity and improving the rate of healing [49]. The same cream formulation penetrated also intact porcine skin and significantly reduced expression of target proteins compared to dosed matched IgG controls [50].

Although the mutant mice used in this study fall short of mimicking the phenotype of human carriers of the Cx30 p.A88V mutation [10,11,13,14], they exhibit hyperproliferation in the skin and its appendages, a feature shared by most Cx-related genodermatoses [5,23,24,45]. Likewise, the Cx26$^{G45E/+}$ mouse model of keratitis-ichthyosis-deafness (KID) syndrome (OMIM #148210) displayed hyperkeratosis, scaling, skin folds, hyperplasia, acanthosis, papillomatosis and increased cell size, as well as increased hemichannel currents in transgenic keratinocytes [72]. Altered epidermal lipid processing and Ca^{2+} distribution were reported also in Cx26$^{S17F/+}$ mice, another
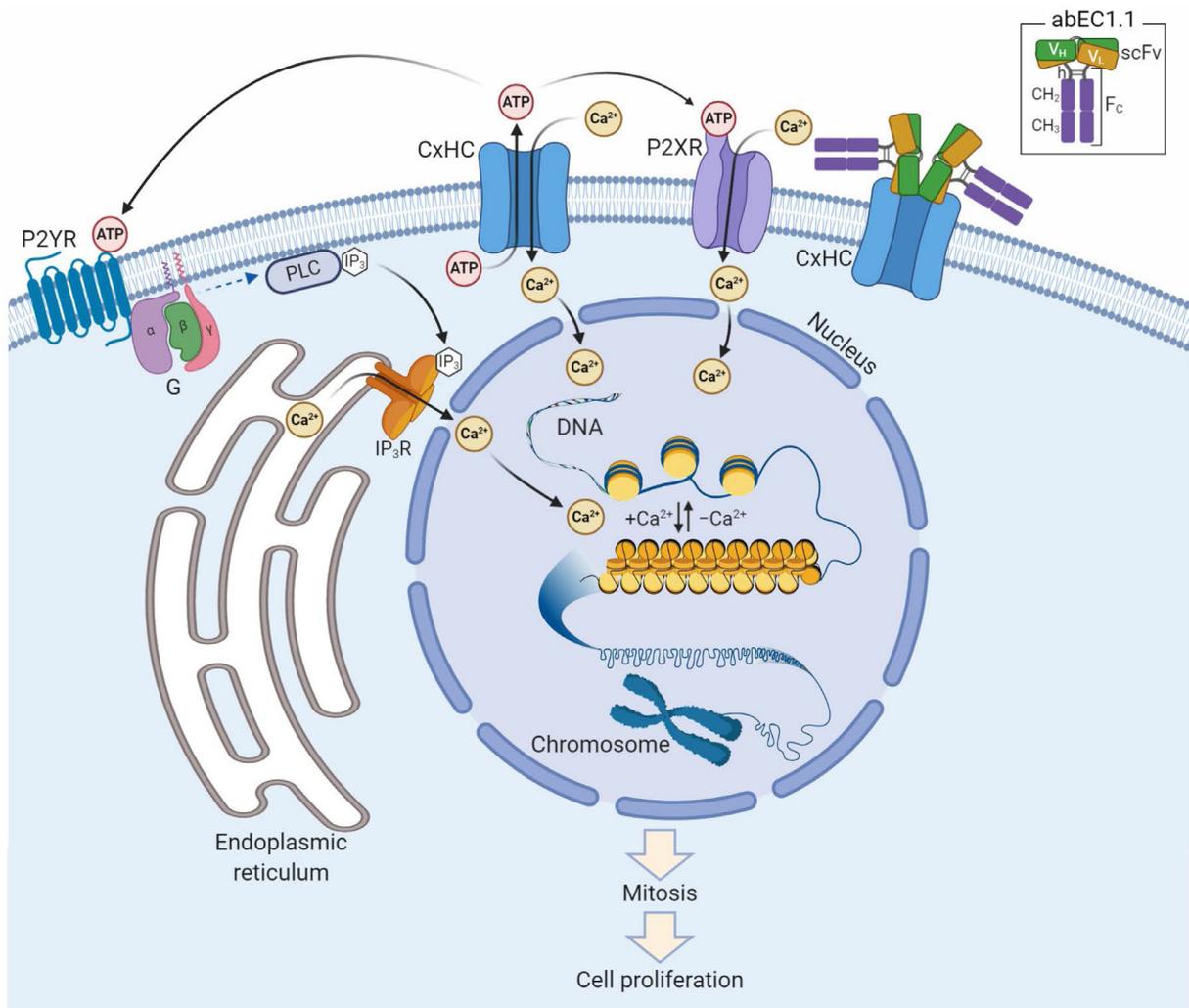
Fig. 7. Schematic representation of putative antibody mechanism of action. abEC1.1 (inset) comprises a Cx-binding scFv complex (V_H-linker-V_L) fused to a fragment constant (Fc) composed of hinge (h), CH_2 and CH_3 domains of secreted IgG1. Two scFv-Fc homodimers bind the outer vestibule of the connexin hemichannel (CxHC) blocking ATP release and Ca^{2+} influx [this work and Refs. [35,36]]. The ATP released by open/unblocked CxHCs [this work and Ref. [10]] diffuses in the extracellular milieu and activates G-protein coupled P2Y receptors (P2YR),[29,30] triggering a canonical signal transduction cascade that leads to Ca^{2+} release from the endoplasmic reticulum via phospholipase C (PLC), PIP_2 (not shown) and IP_3.[66] At the same time, Ca^{2+} flows into the cell through ATP-gated P2X ionotropic receptors (P2XR)[30] and open/unblocked CxHCs (this work). Diffusion of Ca^{2+} in the nucleus promotes transition of chromatin structure from fibrous to globular, chromosome condensation, mitosis and cell proliferation.[64-66]

model for KID syndrome [73], and we have shown previously that abEC1.1 is effective *in vitro* against at least two KID variants of Cx26 [35]. In addition, at least three Cx32 mutations (S85C, D178Y, F235C) causing *Charcot-Marie-Tooth disease, X-linked dominant 1* (CMT1X, OMIM #302800), a demyelinating peripheral neuropathy, produce hemichannels with augmented activity [4] and, possibly, deregulated ATP release [74]. Few therapeutic antibodies address dermatological conditions [49,75,76] or neurodegeneration [77]. Our results suggest abEC1.1 might be effective in both contexts.

Connexin channel function can be also modulated with connexin mimetic peptides [78,79] and, recently, it has been shown that blocking Cx43 hemichannels protects against TNF-induced vascular leakage, hypothermia and eventually mortality [80]. However, the same work concluded that "limitations of the present study are that the peptides used have a short lifetime and low in vivo efficacy" [80].

Connexins have been implicated in a several other pathological conditions, including acute and chronic diseases and injuries such as ischemia−reperfusion injury (IRI), diabetic ulcers and epidermal and corneal wounds. Moreover, genetic studies have undisputedly linked connexins to neuropathies, atrial fibrillation and standstill, cataracts,

leukodystrophy, spastic paraplegia, lymphedema, hearing loss and a variety of inherited skin diseases [1,81]. As demonstrated here, targeting connexins offers the opportunity to test new treatments for currently incurable human pathologies [78,79]. Ongoing research efforts indicate antibodies targeting extracellular domain of Cxs [82] are promising candidates also for diagnostic and cancer therapeutic use [83,84].

Combinatorial antibody libraries [85], with their huge amount of affinity binders [86], coupled with phage display technology [87], are rich sources of modulators for cell surface receptors or membrane channels [88]. The search for new antibodies may develop and unprecedented potential for therapeutic applications, well beyond the realm of rare diseases, as it may benefit tremendously from novel whole-cell screening platforms, based on yeast−mammalian cell interaction, which permit direct selection of antibodies against membrane proteins in native state [88].

In conclusion, we believe this work has widened the scope of therapeutic strategies targeting connexins and encourages further studies to characterize abEC1.1 as a tool to combat diseases caused by abnormally active Cx hemichannels. The demonstrated efficacy of abEC1.1

in reaching and blocking hemichannels *in vivo*, together with its specificity for connexins of the beta subfamily, should stimulate an interest for developing similar antibodies that can modulate selectively other connexin hemichannels.

Funding sources

Author Contributions

Conceptualization, F.M.; Formal analysis, F.M., D.B., F.Z.; Funding acquisition, F.M., G.Y., R.A.L., F.Z.; Investigation, Y.K., V.Z., D.B., G.Z., Fl.M., X.S, Y.L., Y.S.; Methodology, C.P., C.N., M.Q.; Project administration, F.M., G.Y., R.A.L., A.M.S, M.R., F.S.; Resources, F.M., G.Y., R.A.L., F.Z., Y.C., L.L., F.C.; Software, F.M., D.B., F.Z.; Supervision, F.M., G.Y., R.A.L., F.Z., A.M.S., M.R., M.Q.; Visualization, Y.K., V.Z., D.B., G.Z., Fl.M, F.M.; Writing − original draft, F.M.; Writing − review & editing, F.M., A.M.S., F.Z., M.R.,V.Z.

Data and materials availability

All data associated with this study are available in the main text or the Supplementary materials. Computer code used to analyze data is available from the authors.

The crystal structure and the amino acid sequence of the abEC1.1 scFv domain have been deposited in the Protein Data Bank (PDB) under the accession code 5WYM.

Mice are available from INFRAFRONTIER/European Mouse Mutant Archive (ID: 07626; 00323), www.infrafrontier.eu.

Declaration of Competing Interest

Drs. F. Mammano, G. Yang and F. Zonta report a patent: "Fully human antibody specifically inhibiting connexin 26", Inventors: Qu Z, Yang G, Mammano F, Zonta F, International application number: PCT/ CN2016/109847, pending to ShanghaiTech University; and a patent: "Composition and Methods to treat Ectodermal Dysplasia 2, Clouston Type", Inventors: Mammano F, Yang G, Zonta F, International Application No.: PCT/CN2019/088689, International Filing Date: 2019-05-28, pending to ShanghaiTech University. All other Authors have nothing to declare.

Supplementary materials

Supplementary material associated with this article can be found in the online version at doi:10.1016/j.ebiom.2020.102825.

References

[1] Srinivas M, Verselis VK, White TW. Human diseases associated with connexin mutations. Biochimica et biophysica acta 2018;1860(1):192–201.

[2] Lilly E, Sellitto C, Milstone LM, White TW. Connexin channels in congenital skin disorders. Seminars in cell & developmental biology 2016;50:4–12.

[3] Mammano F. Inner Ear Connexin Channels: Roles in Development and Maintenance of Cochlear Function. Cold Spring Harbor perspectives in medicine 2019;9 (7).

[4] Retamal MA, Reyes EP, Garcia IE, Pinto B, Martinez AD, Gonzalez C. Diseases associated with leaky hemichannels. Frontiers in cellular neuroscience 2015;9:267.

[5] Garcia IE, Bosen F, Mujica P, et al. From Hyperactive Connexin26 Hemichannels to Impairments in Epidermal Calcium Gradient and Permeability Barrier in the Keratitis-Ichthyosis-Deafness Syndrome. J Invest Dermatol 2016;136(3):574–83.

[6] Dahl E, Manthey D, Chen Y, et al. Molecular cloning and functional expression of mouse connexin-30,a gap junction gene highly expressed in adult brain and skin. The Journal of biological chemistry 1996;271(30):17903–10.

[7] Kretz M, Maass K, Willecke K. Expression and function of connexins in the epidermis, analyzed with transgenic mouse mutants. European journal of cell biology 2004;83(11-12):647–54.

[8] Kretz M, Euwens C, Hombach S, et al. Altered connexin expression and wound healing in the epidermis of connexin-deficient mice. Journal of cell science 2003;116(Pt 16):3443–52.

[9] Lemaitre G, Sivan V, Lamartine J, et al. Connexin 30, a new marker of hyperproliferative epidermis. The British journal of dermatology 2006;155(4):844–6.

[10] Essenfelder GM, Bruzzone R, Lamartine J, et al. Connexin30 mutations responsible for hidrotic ectodermal dysplasia cause abnormal hemichannel activity. Human molecular genetics 2004;13(16):1703–14.

[11] Lamartine J, Munhoz Essenfelder G, Kibar Z, et al. Mutations in GJB6 cause hidrotic ectodermal dysplasia. Nature genetics 2000;26(2):142–4.

[12] Chen N, Xu C, Han B, et al. G11R mutation in GJB6 gene causes hidrotic ectodermal dysplasia involving only hair and nails in a Chinese family. The Journal of dermatology 2010;37(6):559–61.

[13] Sugiura K, Teranishi M, Matsumoto Y, Akiyama M. Clouston syndrome with heterozygous GJB6 mutation p.Ala88Val and GJB2 variant p.Val27Ile revealing mild sensorineural hearing loss and photophobia. JAMA dermatology 2013;149 (11):1350–1.

[14] Yang R, Hu Z, Kong Q, et al. A known mutation in GJB6 in a large Chinese family with hidrotic ectodermal dysplasia. Journal of the European Academy of Dermatology and Venereology: JEADV 2016;30(8):1362–5.

[15] Berger AC, Kelly JJ, Lajoie P, Shao Q, Laird DW. Mutations in Cx30 that are linked to skin disease and non-syndromic hearing loss exhibit several distinct cellular pathologies. Journal of cell science 2014;127(Pt 8):1751–64.

[16] Boukamp P, Petrussevska RT, Breitkreutz D, Hornung J, Markham A, Fusenig NE. Normal keratinization in a spontaneously immortalized aneuploid human keratinocyte cell line. The Journal of cell biology 1988;106(3):761–71.

[17] Lu Y, Zhang R, Wang Z, et al. Mechanistic effect of the human GJB6 gene and its mutations in HaCaT cell proliferation and apoptosis. Braz J Med Biol Res 2018;51 (9):e7560.

[18] Koster MI. Making an epidermis. Annals of the New York Academy of Sciences 2009;1170:7–10.

[19] Fuchs E. Chapter Nineteen - Epithelial Skin Biology: Three Decades of Developmental Biology, a Hundred Questions Answered and a Thousand New Ones to Address. In: Wassarman PM, editor. Current Topics in Developmental Biology. Academic Press; 2016. p. 357–74.

[20] Hennings H, Michael D, Cheng C, Steinert P, Holbrook K, Yuspa SH. Calcium regulation of growth and differentiation of mouse epidermal cells in culture. Cell 1980;19(1):245–54.

[21] Elsholz F, Harteneck C, Muller W, Friedland K. Calcium−a central regulator of keratinocyte differentiation in health and disease. European journal of dermatology: EJD 2014;24(6):650–61.

[22] Michaletti A, Mancini M, Smirnov A, Candi E, Melino G, Zolla L. Multi-omics profiling of calcium-induced human keratinocytes differentiation reveals modulation of unfolded protein response signaling pathways. Cell cycle 2019;18(17):2124–40.

[23] Martin PE, van Steensel M. Connexins and skin disease: insights into the role of beta connexins in skin homeostasis. Cell and tissue research 2015;360(3):645–58.

[24] Laird DW, Naus CC, Lampe PD. SnapShot: Connexins and Disease. Cell 2017;170 (6) 1260- e1.

[25] Burrell HE, Wlodarski B, Foster BJ, et al. Human keratinocytes release ATP and utilize three mechanisms for nucleotide interconversion at the cell surface. The Journal of biological chemistry 2005;280(33):29667–76.

[26] Barr TP, Albrecht PJ, Hou Q, Mongin AA, Strichartz GR, Rice FL. Air-stimulated ATP release from keratinocytes occurs through connexin hemichannels. PloS one 2013;8(2):e56744.

[27] Takahashi T, Kimura Y, Niwa K, et al. In vivo imaging demonstrates ATP release from murine keratinocytes and its involvement in cutaneous inflammation after tape stripping. J Invest Dermatol 2013;133(10):2407–15.

[28] Takada H, Furuya K, Sokabe M. Mechanosensitive ATP release from hemichannels and Ca(2)(+) influx through TRPC6 accelerate wound closure in keratinocytes. Journal of cell science 2014;127(Pt 19):4159–71.

[29] Lee WK, Choi SW, Lee HR, Lee EJ, Lee KH, Kim HO. Purinoceptor-mediated calcium mobilization and proliferation in HaCaT keratinocytes. Journal of dermatological science 2001;25(2):97–105.

[30] Burnstock G, Knight GE, Greig AV. Purinergic signaling in healthy and diseased skin. J Invest Dermatol 2012;132(3 Pt 1):526–46.

[31] Bosen F, Schutz M, Beinhauer A, Strenzke N, Franz T, Willecke K. The Clouston syndrome mutation connexin30 A88V leads to hyperproliferation of sebaceous glands and hearing impairments in mice. FEBS letters 2014;588(9):1795–801.

[32] Horsley V, O'Carroll D, Tooze R, et al. Blimp1 defines a progenitor population that governs cellular input to the sebaceous gland. Cell 2006;126(3):597–609.

[33] Kelly JJ, Abitbol JM, Hulme S, Press ER, Laird DW, Allman BL. The connexin 30 A88V mutant reduces cochlear gap junction expression and confers long-term protection against hearing loss. Journal of cell science 2019;132(2).

[34] Lukashkina VA, Levic S, Lukashkin AN, Strenzke N, Russell IJ. A connexin30 mutation rescues hearing and reveals roles for gap junctions in cochlear amplification and micromechanics. Nature communications 2017;8:14530.

[35] Xu L, Carrer A, Zonta F, et al. Design and Characterization of a Human Monoclonal Antibody that Modulates Mutant Connexin 26 Hemichannels Implicated in Deafness and Skin Disorders. Frontiers in molecular neuroscience 2017;10:298.

[36] Ziraldo G, Buratto D, Kuang Y, et al. A Human-Derived Monoclonal Antibody Targeting Extracellular Connexin Domain Selectively Modulates Hemichannel Function. Frontiers in physiology 2019;10:392.

[37] Singh S, Kumar N, Dwiwedi P, et al. Monoclonal Antibodies: A Review. Current clinical pharmacology 2017.

[38] Carter PJ, Lazar GA. Next generation antibody drugs: pursuit of the 'high-hanging fruit'. Nat Rev Drug Discov 2018;17(3):197–223.

[39] Perisic O, Webb PA, Holliger P, Winter G, Williams RL. Crystal structure of a diabody, a bivalent antibody fragment. Structure 1994;2(12):1217–26.

[40] Bujak E, Matasci M, Neri D, Wulfhard S. Reformatting of scFv antibodies into the scFv-Fc format and their downstream purification. Methods in molecular biology 2014;1131:315–34.

[41] Butterweck A, Elfgang C, Willecke K, Traub O. Differential expression of the gap junction proteins connexin45, -43, -40, -31, and -26 in mouse skin. European journal of cell biology 1994;65(1):152–63.

[42] Salomon D, Masgrau E, Vischer S, et al. Topography of mammalian connexins in human skin. J Invest Dermatol 1994;103(2):240–7.

[43] Goliger JA, Paul DL. Expression of gap junction proteins Cx26, Cx31.1, Cx37, and Cx43 in developing and mature rat epidermis. Developmental dynamics: an official publication of the American Association of Anatomists 1994;200(1):1–13.

[44] Di WL, Rugg EL, Leigh IM, Kelsell DP. Multiple epidermal connexins are expressed in different keratinocyte subpopulations including connexin 31. J Invest Dermatol 2001;117(4):958–64.

[45] Faniku C, Wright CS, Martin PE. Connexins and pannexins in the integumentary system: the skin and appendages. Cellular and molecular life sciences: CMLS 2015;72(15):2937–47.

[46] Vidarsson G, Dekkers G, Rispens T. IgG subclasses and allotypes: from structure to effector functions. Frontiers in immunology 2014;5:520.

[47] Kilkenny C, Browne WJ, Cuthill IC, Emerson M, Altman DG. Improving bioscience research reporting: the ARRIVE guidelines for reporting animal research. PLoS biology 2010;8(6) e1000412.

[48] Smith AJ, Clutton RE, Lilley E, Hansen KEA, Brattelid T. PREPARE: guidelines for planning animal research and testing. Laboratory animals 2018;52(2):135–41.

[49] Kopecki Z, Ruzehaji N, Turner C, et al. Topically applied flightless I neutralizing antibodies improve healing of blistered skin in a murine model of epidermolysis bullosa acquisita. J Invest Dermatol 2013;133(4) 1008-16.

[50] Haidari H, Zhang Q, Melville E, et al. Development of Topical Delivery Systems for Flightless Neutralizing Antibody. Journal of pharmaceutical sciences 2017;106(7) 1795-804.

[51] Engvall E, Perlmann P. Enzyme-linked immunosorbent assay, Elisa. 3. Quantitation of specific antibodies by enzyme-labeled anti-immunoglobulin in antigen-coated tubes. J Immunol 1972;109(1) 129-35.

[52] Lohman AW, Isakson BE. Differentiating connexin hemichannels and pannexin channels in cellular ATP release. FEBS letters 2014;588(8):1379–88.

[53] Li F, Adase CA, Zhang LJ. Isolation and Culture of Primary Mouse Keratinocytes from Neonatal and Adult Mouse Skin. Journal of visualized experiments: JoVE 2017(125).

[54] Westfall TD, Kennedy C, Sneddon P. Enhancement of sympathetic purinergic neurotransmission in the guinea-pig isolated vas deferens by the novel ecto-ATPase inhibitor ARL 67156. British journal of pharmacology 1996;117(5):867–72.

[55] Fasciani I, Temperan A, Perez-Atencio LF, et al. Regulation of connexin hemichannel activity by membrane potential and the extracellular calcium in health and disease. Neuropharmacology 2013.

[56] Lane DM, Scott D, Hebl M, Guerra R, Osherson D, Zimmer H. Introduction to Statistics. Open Textbook Library; 2003. p. 473 http://onlinestatbook.com/.

[57] Kamath AV. Translational pharmacokinetics and pharmacodynamics of monoclonal antibodies. Drug discovery today Technologies 2016;21-22:75–83.

[58] Unverdorben F, Richter F, Hutt M, et al. Pharmacokinetic properties of IgG and various Fc fusion proteins in mice. mAbs 2016;8(1):120–8.

[59] Greenspan P, Mayer EP, Fowler SD. Nile red: a selective fluorescent stain for intracellular lipid droplets. The Journal of cell biology 1985;100(3):965–73.

[60] Tucci MG, Offidani A, Lucarini G, et al. Advances in the understanding of malignant transformation of keratinocytes: an immunohistochemical study. Journal of the European Academy of Dermatology and Venereology: JEADV 1998;10 (2):118–24.

[61] Valiunas V, Weingart R. Electrical properties of gap junction hemichannels identified in transfected HeLa cells. Pflugers Archiv: European journal of physiology 2000;440(3):366–79.

[62] Rasmussen CD, Means AR. Calmodulin is required for cell-cycle progression during G1 and mitosis. The EMBO journal 1989;8(1):73–82.

[63] Salisbury JL, Suino KM, Busby R, Springett M. Centrin-2 is required for centriole duplication in mammalian cells. Current biology: CB 2002;12(15):1287–92.

[64] Phengchat R, Takata H, Morii K, et al. Calcium ions function as a booster of chromosome condensation. Scientific reports 2016;6:38281.

[65] Helassa N, Nugues C, Rajamanoharan D, Burgoyne RD, Haynes LP. A centrosome-localized calcium signal is essential for mammalian cell mitosis. FASEB journal: official publication of the Federation of American Societies for Experimental Biology 2019;33(12):14602–10.

[66] Giorgi C, Danese A, Missiroli S, Patergnani S, Pinton P. Calcium Dynamics as a Machine for Decoding Signals. Trends in cell biology 2018;28(4):258–73.

[67] Ransford GA, Fregien N, Qiu F, Dahl G, Conner GE, Salathe M. Pannexin 1 contributes to ATP release in airway epithelia. American journal of respiratory cell and molecular biology 2009;41(5):525–34.

[68] Sridharan M, Adderley SP, Bowles EA, et al. Pannexin 1 is the conduit for low oxygen tension-induced ATP release from human erythrocytes. American journal of physiology Heart and circulatory physiology 2010;299(4):H1146–52.

[69] Dolmatova E, Spagnol G, Boassa D, et al. Cardiomyocyte ATP release through pannexin 1 aids in early fibroblast activation. American journal of physiology Heart and circulatory physiology 2012;303(10):H1208–18.

[70] Sandilos JK, Chiu YH, Chekeni FB, et al. Pannexin 1, an ATP release channel, is activated by caspase cleavage of its pore-associated C-terminal autoinhibitory region. The Journal of biological chemistry 2012;287(14):11303–11.

[71] Wang J, Jackson DG, Dahl G. Cationic control of Panx1 channel function. American journal of physiology Cell physiology 2018;315(3):C279–C89.

[72] Mese G, Sellitto C, Li L, et al. The Cx26-G45E mutation displays increased hemichannel activity in a mouse model of the lethal form of keratitis-ichthyosis-deafness syndrome. Molecular biology of the cell 2011;22(24):4776–86.

[73] Bosen F, Celli A, Crumrine D, et al. Altered epidermal lipid processing and calcium distribution in the KID syndrome mouse model Cx26S17F. FEBS letters 2015;589 (15):1904–10.

[74] Bortolozzi M. What's the Function of Connexin 32 in the Peripheral Nervous System. Frontiers in molecular neuroscience 2018;11:227.

[75] Beck LA, Thaci D, Hamilton JD, et al. Dupilumab treatment in adults with moderate-to-severe atopic dermatitis. The New England journal of medicine 2014;371 (2):130–9.

[76] Puig L. Guselkumab for the treatment of adults with moderate to severe plaque psoriasis. Expert Rev Clin Immunol 2019;15(6):589–97.

[77] Courade JP, Angers R, Mairet-Coello G, et al. Epitope determines efficacy of therapeutic anti-Tau antibodies in a functional assay with human Alzheimer Tau. Acta neuropathologica 2018;136(5):729–45.

[78] Laird DW, Lampe PD. Therapeutic strategies targeting connexins. Nat Rev Drug Discov 2018;17:905.

[79] Delvaeye T, Vandenabeele P, Bultynck G, Leybaert L, Krysko DV. Therapeutic Targeting of Connexin Channels: New Views and Challenges. Trends in molecular medicine 2018;24(12):1036–53.

[80] Delvaeye T, De Smet MAJ, Verwaerde S, et al. Blocking connexin43 hemichannels protects mice against tumour necrosis factor-induced inflammatory shock. Scientific reports 2019;9(1):16623.

[81] Saez JC, Leybaert L. Hunting for connexin hemichannels. FEBS letters 2014;588 (8):1205–11.

[82] Riquelme MA, Kar R, Gu S, Jiang JX. Antibodies targeting extracellular domain of connexins for studies of hemichannels. Neuropharmacology 2013;75:525–32.

[83] Yusubalieva GM, Baklaushev VP, Gurina OI, et al. Treatment of Poorly Differentiated Glioma Using a Combination of Monoclonal Antibodies to Extracellular Connexin-43 Fragment, Temozolomide, and Radiotherapy. B Exp Biol Med+ 2014;157 (4):510–5.

[84] Jiang JX, An Z, Zhang N, et al., inventors; Connexin (cx) 43 hemichannel-binding antibodies and uses thereof. USA patent US 20190359696Al. 2019 Nov. 28, 2019.

[85] Lerner RA. Combinatorial antibody libraries: new advances, new immunological insights. Nature reviews Immunology 2016;16(8):498–508.

[86] Frenzel A, Kugler J, Wilke S, Schirrmann T, Hust M. Construction of human antibody gene libraries and selection of antibodies by phage display. Methods in molecular biology 2014;1060:215–43.

[87] McCafferty J, Griffiths AD, Winter G, Chiswell DJ. Phage antibodies: filamentous phage displaying antibody variable domains. Nature 1990;348(6301):552–4.

[88] Yang Z, Wan Y, Tao P, et al. A cell-cell interaction format for selection of high-affinity antibodies to membrane proteins. Proceedings of the National Academy of Sciences of the United States of America 2019;116(30):14971–8.